
This is an electronic reprint of the original article.
This reprint may differ from the original in pagination and typographic detail.

Karki, Sabin Kumar; Ala-Laurinaho, Juha; Viikari, Ville; Valkonen, Risto

Effect of mutual coupling between feed elements on integrated lens antenna performance

Published in:
IET Microwaves Antennas and Propagation

DOI:
[10.1049/iet-map.2017.1082](https://doi.org/10.1049/iet-map.2017.1082)

Published: 15/08/2018

Document Version
Peer-reviewed accepted author manuscript, also known as Final accepted manuscript or Post-print

Please cite the original version:
Karki, S. K., Ala-Laurinaho, J., Viikari, V., & Valkonen, R. (2018). Effect of mutual coupling between feed elements on integrated lens antenna performance. *IET Microwaves Antennas and Propagation*, 12(10), 1649-1655. <https://doi.org/10.1049/iet-map.2017.1082>

This material is protected by copyright and other intellectual property rights, and duplication or sale of all or part of any of the repository collections is not permitted, except that material may be duplicated by you for your research use or educational purposes in electronic or print form. You must obtain permission for any other use. Electronic or print copies may not be offered, whether for sale or otherwise to anyone who is not an authorised user.

Effect of mutual coupling between feed elements on Integrated Lens Antenna performance

Sabin Kumar Karki^{1*}, Juha Ala-Laurinaho¹, Ville Viikari¹, Risto Valkonen²

¹ Department of Electronics and Nanoengineering, Aalto University, Maarintie 8, Espoo, Finland

² Nokia Bell-Labs, Karaportti 3, Espoo, Finland

* E-mail: sabin.karki@aalto.fi

Abstract: An integrated lens antenna (ILA) equipped with a beam-switching array feed provides beam steering. This paper investigates the effects of the mutual coupling between the feed array elements on the ILA performance. A simulation study of an ILA with two different feed types with varying mutual coupling levels is done. Radiation pattern and boresight directivity of the ILA are in the prime focus of the study. An aperture coupled microstrip patch antenna (ACMPA) and a stacked ACMPA feeds embedded in an array are used to study the radiation characteristics of the ILA. Results show that changes in directivity and radiation pattern of the feed caused by the mutual coupling has significant impact in the ILA characteristics. However, it is found that the mutual coupling level alone does not predict well the changes in the ILA radiation. Among two feed antenna types with similar mutual coupling variation, the stacked ACMPA feed with less boresight radiation pattern distortion gives better ILA performance compared to the ACMPA feed with significant boresight radiation pattern distortion. Furthermore, impact of the port impedance mismatch of the adjacent inactive antennas on the active element performance of a beam-switching feed network and its corresponding impact on the ILA is investigated.

1 Introduction

Increasing use of higher frequencies, low fabrication cost, easily available dielectric materials, and modern fabrication technologies has fostered the use of lens antennas in telecommunications, automotive radars, and imaging applications. High gain and beam steering ability of a lens antenna makes it even more relevant for millimeter-wave communications systems.

An integrated lens antenna (ILA) with a beam-switching array feed at the focal plane has been studied before for the beam-steering properties, e.g. in [1] [2] [3]. Mutual coupling between closely placed array elements is inevitable. Mutual coupling is typically undesirable because of its impact on the array impedance, radiation pattern, and efficiency. Moreover, the gain of an ILA is proportional to the feed directivity because the higher directivity reduces the spillover loss [4]. The directivity of a feed antenna is directly proportional to its aperture area. The feed element spacing in an array is determined by the far-field beam-overlapping requirement. For efficient and reliable communication link higher cross-over levels of the overlapping beams are desired which demands for smaller feed separation distance. The stringent requirements of ILA beam-overlapping and feed directivity leads to larger mutual coupling in a beam-switching array. Thus, it becomes important to understand the effects of the feed's mutual coupling on the ILA characteristics. Mutual coupling between antenna array elements have been extensively studied, see e.g. [5] [6], where all elements are excited simultaneously. However, a beam-switching array differs because single feed element is excited at given moment of time. To our knowledge, in the previous ILA studies, the mutual coupling analysis between beam-switching array elements and in particular its effects on the ILA performance are not comprehensively investigated.

In practice, a beam-switching array is placed in the focal plane of an ILA to achieve electronic beam-steering [3]. RF switches are used to excite a single feed element in an array structure. Active port (i.e. switched ON port) impedance of the RF switches is considered to be matched with characteristic impedances but the impedance seen at the remaining inactive ports (i.e. switched OFF) may be far from matched condition. Mismatch in the port impedance of the adjacent

antennas may affect the active feed antenna and consequently the ILA performance. Therefore, it becomes essential to study the effect of such mismatch for precise lens performance estimation.

The paper investigates ILA characteristics with respect to varying feed mutual coupling and port impedances through simulations. Directivity, radiation pattern, gain, and beam-steering properties are mainly observed. In-house ray-tracing program is used to study the 160-mm ILA characteristics with respect to two different types of embedded feed arrays with varying mutual coupling levels and port impedances [4]. Far-field radiation patterns of the ACMPA and the stacked ACMPA simulated in the CST electromagnetic simulator are used as the feeds in the ray-tracing program. The aperture field pattern and far-field radiation pattern of the ILA using two different types of feeds with similar mutual coupling variations are analysed to derive conclusions. In this work, designs and analysis are done for 73.5 GHz, however conclusions are expected to be valid in other frequency ranges as well.

This paper is divided into following sections: section 2 presents the related theory and research methodology; in section 3, two different types of feed array are designed and their characteristics are presented; in section 4, ILA performance with these two different feeds are presented; impact of the port mismatch is studied in section 5; and finally in section 6, discussion and recommendations regarding the feed array designs are presented and it is followed by conclusion and acknowledgement.

2 Background and methods

It is well known that the maximum boresight gain for an ILA can be achieved with an elliptical collimating surface [7]. Optimum focusing properties of an ILA can be achieved with design guidelines described in [8]. Other forms of ILA may be useful in different applications, e.g. extended hemispherical lens can be used to improve beam-steering properties [9]. Eccentricity of the elliptical ILA is inversely proportional to the square root of relative permittivity ϵ_r of the lens material i.e. $e = \frac{1}{\sqrt{\epsilon_r}}$. Length L of the extension section should be equal to product of eccentricity e and major axis a of the

elliptical collimating part of the lens (i.e. $L = e \cdot a$). The minor axis of the elliptical surface and the aperture surface radius is denoted by b .

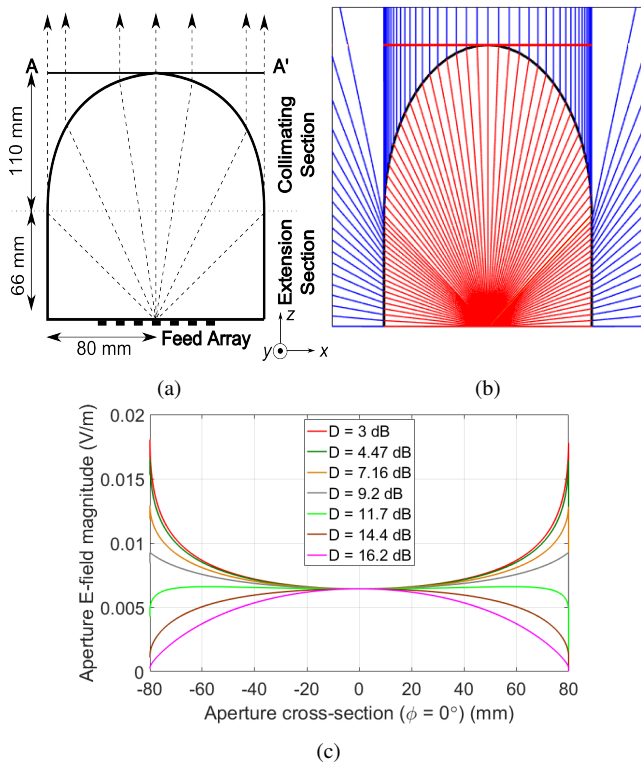


Fig. 1: (a) 2D shape, (b) ray presentation, and (c) magnitude of aperture (AA') field distribution of the elliptical ILA made of Polyethylene ($\epsilon_r = 2.31$ and $\tan\delta = 0.0003$). Feed directivity is varied for the aperture field.

Ray-tracing method is used in designing and characterizing electrically large structures like lens and reflector antennas to minimize high processing and memory requirement of the full-wave methods. Rays from the feed antenna are shot in equal angular interval. Then, the laws of straight line propagation in homogenous region is used to trace ray propagation to the lens-air interface. Incident electric field, polarization vectors, and the Snell's law is used to calculate the field on the lens-air interface. Then the field \vec{E}_a at the aperture surface close to the ILA is calculated. The calculated aperture field is transformed to far-field using aperture integration of equivalent surface currents [10]. Only the rays emitting from the collimating section are considered during far-field calculation. This is reasonable as in practice, absorbers can be placed along the extension section to terminate the rays exiting from the extension section to improve boresight directivity and to minimize sidelobe level [3]. In [11], the angular domain of the ILA collimating surface has been categorized and its impact on the radiation properties and input admittance has been studied. As the low permittivity material used for the ILA design, the effects of higher order reflections is not considered in this work.

The aperture field distribution of the 160-mm ILA fed with an ideal point source radiation pattern is presented in Figure 1 (c). The point source feed radiation pattern is defined as

$$E(\phi, \theta) = \cos^N(\theta), \quad (1)$$

where $0^\circ < \theta < 90^\circ$, $0^\circ < \phi < 360^\circ$, and the directivity of the source varies with parameter N . In this analysis, parameter N is varied from 0 to 10, consequently the directivity is varied from 3.0 dB to 16.2 dB. Aperture field amplitude at $\theta = 0^\circ$ is equal for all feed directivity i.e. 1 for all values of N . The 160-mm ILA similar

to [4], is used for the simulations in this work. The ILA is designed with Polyethylene ($\epsilon_r = 2.31$ and $\tan\delta = 0.0003$) material. Magnitude distribution of the aperture field at AA' are shown in Figure 1 (c). Since the maximum directivity of a uniform phased aperture is obtained with an uniform amplitude aperture, the maximum ILA directivity is obtained with feed directivity of 11.7 dB [12]. However, this though is not optimum for the gain performance. Although, the ILA directivity decreases after the 11.7-dB feed directivity at the same time the spillover loss decreases that helps to improve the gain performance. Therefore, the optimum feed directivity for the ILA gain is between 13-14 dB [4].

The amplitude of the aperture field for low directivity feed (i.e. < 11.7 dB) is higher towards the edges due to large number of rays hitting edges of the surface as shown in Figure 1 (b). Once the feed becomes more directive (i.e. > 11.7 dB), amplitude is greater towards the center of the aperture surface. This is due to under illumination of the lens collimating surface towards the edge. For the aperture surface AA' of the 160-mm ILA fed with ideal point source, the aperture phase pattern for all feed directivity is equi-phased.

3 Feed array

Due to ease of integration with the RF circuit and low back radiation make an aperture coupled microstrip patch antenna (ACMPA) array a viable option for an ILA feed. The directivity of the ACMPA can be improved by increasing the effective aperture area, e.g., by adding the parasitic patches in stacked configuration [13]. This method increases the mutual coupling between the feed elements [14]. Therefore, ACMPA and stacked ACMPA are used as array elements in this work.

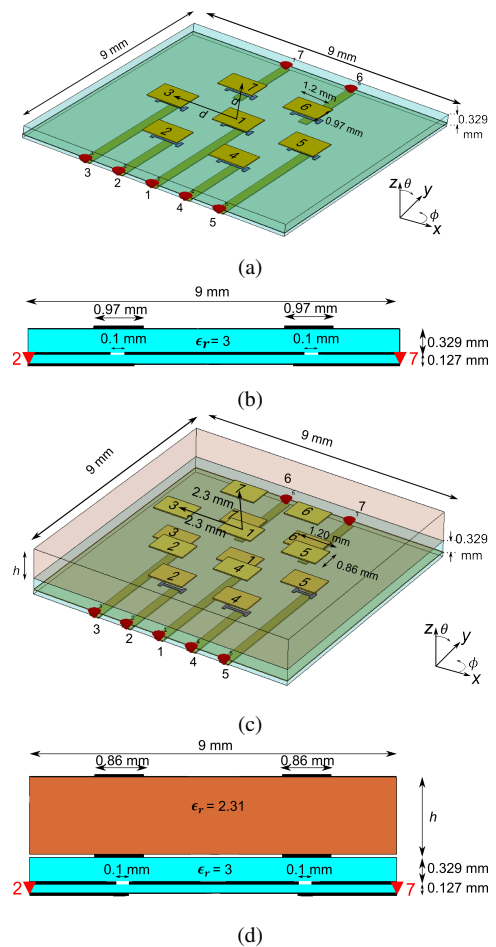


Fig. 2: Orthographic and yz-plane cross section views at $x = -1.15$ mm for the embedded ACMPA (EA) (a) and (b), and Embedded Stacked ACMPA (ESA) (c) and (d).

The ACPMA and stacked ACPMA are embedded in an array configuration with surrounding identical antenna elements in 9×9 mm ASTRA substrate ($\epsilon_r = 3$ and $\tan\delta = 0.0014$) as shown in Figure 2. At a given time, only one element within the array configuration is excited (i.e. center element 1 for both arrays in this work), hence it is referred as an embedded structure. The embedded ACPMA (EA) and embedded stacked ACPMA (ESA) are designed with various level of mutual coupling. Basic geometry of the ACPMA used in both array structures is similar to the one designed in [15]. Orthographic view and yz-plane cut at $x = -1.15$ mm of both embedded structures are shown in Figure 2 (a), (b), (c) and (d). It is important to note that the structures are not fully symmetrical as the microstrip transmission lines of element 6 and 7 are in opposite direction w.r.t. to remaining elements. Polyethylene is used as the background material in simulations to accurately estimate feed performance in the presence of the Polyethylene ILA. The Polyethylene material is also used as the superstrate material in between the radiating and parasitic patches of the ESA.

The dimensions of the array elements of both structures are designed to operate in lower E-band i.e. 71-76 GHz. Originally, both embedded arrays are optimized with element separation distance $d = 2.3$ mm to meet -3 dB beam overlapping criteria in the ILA farfield. In traditional rectangular arrangement, the separation distance along the diagonal elements is more than along the axis elements. Hence, the far-field overlapping occurs at level lower than -3 dB. Therefore, feed elements are arranged as shown in Figure 2, where each elements surrounding the center element are place at equal distance. Therefore, this arrangement has been chosen. The impedance bandwidth ($|S_{11}| < -10$ dB) is approximately 3 GHz and more than 6 GHz for the EA and ESA feed respectively, with $d = 2.3$ mm and $h = 0.85$ mm. Radiation pattern of both feeds remains similar in entire frequency band. It is worth to note that the feed arrays are designed to achieve varying level of mutual coupling rather than to maximize directivity or bandwidth.

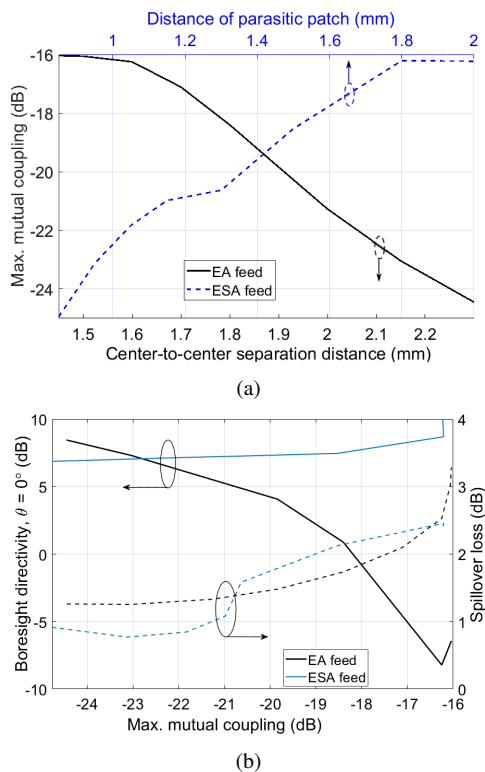


Fig. 3: (a) Mutual coupling levels with varying d and h (b) boresight directivity $\theta = 0^\circ$ w.r.t. mutual coupling of both feeds.

The element separation distance d of the EA is varied between 2.3 mm and 1.45 mm to create various levels of mutual coupling. In case of the ESA, distance of the parasitic patch h is varied between

0.85 mm and 2 mm while keeping the element separation distance as 2.3 mm. As expected, with decreasing center-to-center separation distance d mutual coupling of the EA increases, and the mutual coupling between ESA elements increases with increasing the parasitic patch distance h , see Figure 3 (a). Mutual coupling variation for both the EA and the ESA is similar, i.e. from -25 dB to -16 dB for d and h sweep, respectively. Figure 3 (b) and 4 illustrates that the amount of radiation pattern distortion of the feed as the function of maximum mutual coupling which is defined as $\max |S_{n1}|$, where $n = 2, 3 \dots 7$.

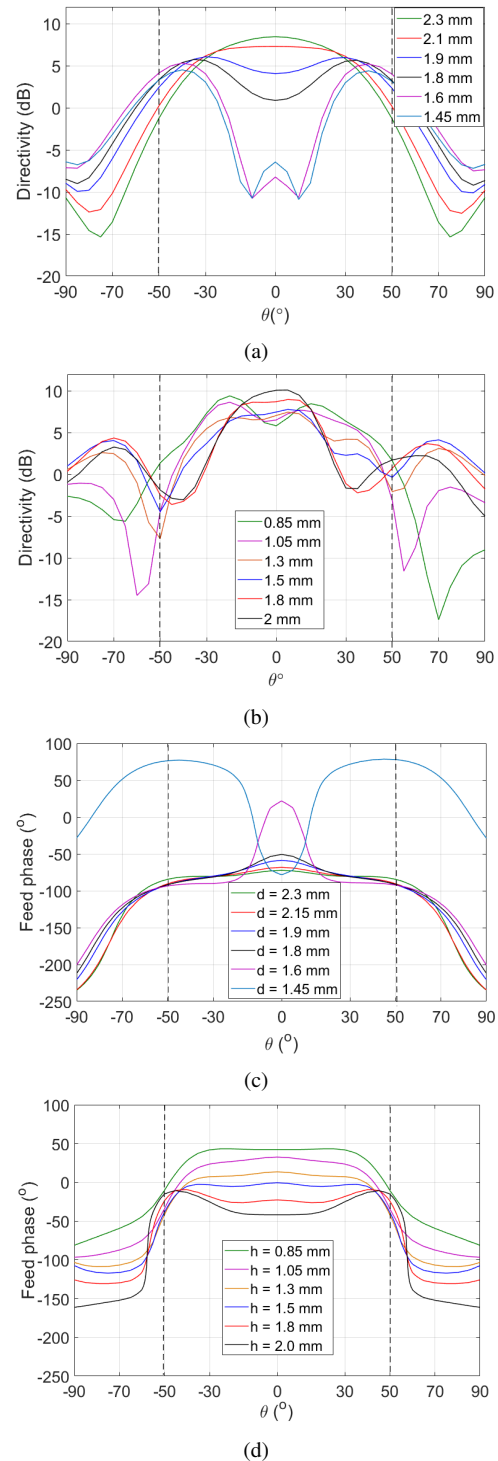


Fig. 4: Directivity of the (a) EA and (b) ESA feed, and far-field phase pattern of the (c) EA and (d) ESA feed in the $\phi = 0^\circ$ (H-plane) cut. Dashed lines show the approximate angular extent of the collimating part.

The radiation pattern of the antenna element in an embedded configuration starts to distort due to higher mutual coupling. Directivity pattern of the EA and the ESA with varying mutual coupling at H-plane cut ($\phi = 0^\circ$) is shown in Figure 4 (a) and (b), respectively. Significant distortion of the main beam of the EA occurs when the element separation $d < 1.9$ mm. With decreasing separation distance, unequal power coupling across elements 2/4 and 6/7 increases that leads to larger distortions and the main lobe is directed towards elements 6 and 7. With equal element separation distance of 1.45 mm, the maximum mutual coupling is approximately -16 dB in elements 6/7 and the coupling in element 2/4 is 9 dB lower. Non-symmetrical nature of the embedded structure as mentioned earlier could be plausible reason for uneven coupling between feed elements and radiation pattern distortion. Hence, the main lobe is directed towards $\theta = 45^\circ$ and boresight directivity at $\theta = 0^\circ$ is as low as -10 dB, see Figure 3 (b). However, it is important to note that the spillover loss increases only couple of dBs. In case of the ESA, there is no significant distortion of the radiation pattern with increasing parasitic patch distance. As the mutual coupling grows stronger with increasing h , minor increase in sidelobe level can be observed in Figure 4 (b).

Ideally, spherical phase front is expected from the feed element for the optimum ILA performance. However, in an array configuration also phase pattern is distorted due to mutual coupling. Phase pattern of both embedded elements deviates from the expected spherical phase front as shown in Figure 4 (c) and (d). The EA shows larger phase variation within $\pm 50^\circ$ as compared to ESA. Feed radiation towards larger angles than approximately $\pm 50^\circ$ will hit the extension section of the ILA. As stated earlier, only field through the collimating section is considered during far-field calculation. Therefore, phase variation at higher θ angle does not make difference in the ILA radiation pattern calculation.

4 Lens Performance

The previously presented simulated radiation patterns of the EA and the ESA with varying mutual coupling levels are used in the ray-tracing program to feed the 160-mm elliptical ILA. Two dimensional shape of the ILA with aperture surface and rays with on-axis feed is shown in Figure 1 (a) and (b). The variation of the aperture field magnitude in H-plane ($\phi = 0^\circ$) with the EA and the ESA feed is shown in Figure 5 (a) and (b), respectively. With the EA feed, the aperture field magnitude of the ILA decreases with the smaller separation distance d . The figure illustrates the decreased illumination of the ILA collimating surface. Decreasing separation distance between the EA elements increases mutual coupling and severely distorts the radiation pattern of the feed. Instead, in case of the ESA feed, the aperture field magnitude does not decrease with increasing mutual coupling. Figures 4 and 5 indicate that the ILA aperture field distribution depends more on the radiation pattern of the feed rather than the peak directivity and the mutual coupling between embedded elements.

Under ideal condition the aperture field should be equi-phased. Aperture field of the ILA fed by EA feed with low mutual coupling is almost equi-phased. For EA feed, as the mutual coupling increases and the feed radiation pattern changes, the phase distribution along the aperture surface starts to distort as shown in Figure 5 (a). The comparison between Figure 5 (a) and (c) with d equal to 1.6 mm and 1.45 mm highlights the dependence of the ILA directivity on the aperture phase distribution. In case of the ESA feed, aperture field of the ILA is almost equi-phased for all the levels of feed mutual coupling.

Due to the distortions in the radiation pattern both in magnitude and phase of the EA, the ILA directivity decreases and the side lobe level (SLL) increases with the increasing mutual coupling as shown in Figure 5 (c). In case of the ESA feed, though the mutual coupling varies in range similar to that of the EA, yet there is minimum effect upon the ILA directivity because of the minimum distortion of the feed radiation pattern. For maximum mutual coupling level of -16 dB in the EA and the ESA feed, the boresight directivity of the ILA is 36.9 dB and 41.5 dB, respectively. Directivity radiation pattern of

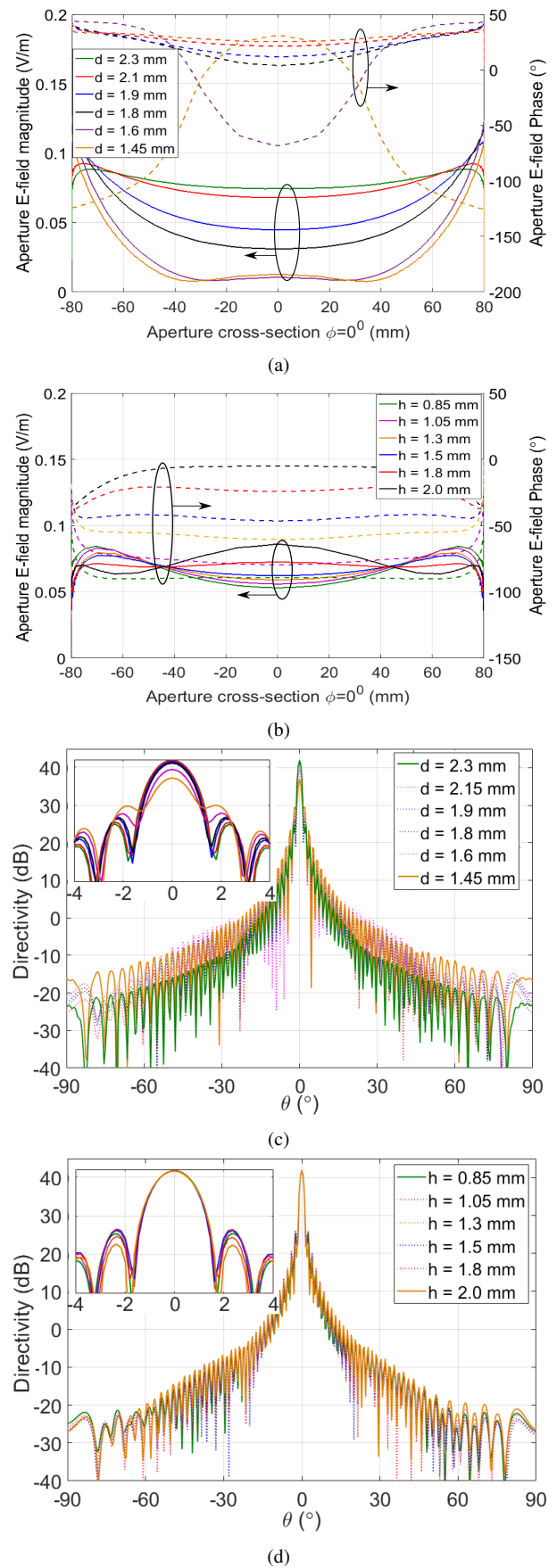


Fig. 5: Amplitude and phase distribution at the aperture surface of the ILA with (a) EA and (b) ESA array feed, and ILA directivity pattern of the (c) EA and (d) ESA feed in the $\phi = 0^\circ$ (H-plane) cut with varying mutual coupling level i.e. with varying element separation d and parasitic patch distance h , respectively.

the 160-mm ILA, fed with EA and ESA is shown in Figure 5 (c) and (d), respectively.

In case of the EA and ESA feed, with the increasing feed mutual coupling the spillover loss and total loss of the ILA increases for both feed types. However, this relation between spillover loss and mutual coupling cannot be generalized for other feed types, as the effect of mutual coupling on the feed radiation pattern distortion is unknown. Gain of the ILA worsens due to combined effect of decreasing directivity and increasing loss as shown in Figure 6 (a). Another important aspect is that the ESA directivity and gain decreases despite of higher boresight feed directivity i.e. at $\theta = 0^\circ$. Decrease in the ILA directivity is due to decreased illumination at edges of the collimating surface as the spillover loss increases, see 5 (b). The increase in spillover loss indicates the distortion of the feed pattern, which decreases the illumination of collimating surface and consequently the ILA directivity decreases. For both feeds, the spillover loss shows close correlation with the directivity and gain of ILA.

Similarly, beam-steering properties of the ILA are studied by moving the embedded feed away from the focal point. The feed is placed at 9.2 mm offset position in the ray-tracing simulation. Directivity scan loss performances for the resulting 5.4° -beam angle with the varying mutual coupling of the feed are presented in Figure 6 (b). With both feed types, the scanloss increases with increasing mutual coupling. However, the rate of increase of directivity scanloss of the EA feed with respect to increasing mutual coupling is greater compared to ESA feed. Decreased illumination of the ILA due to distorted radiation pattern of the EA feed is main reason for increased scanloss.

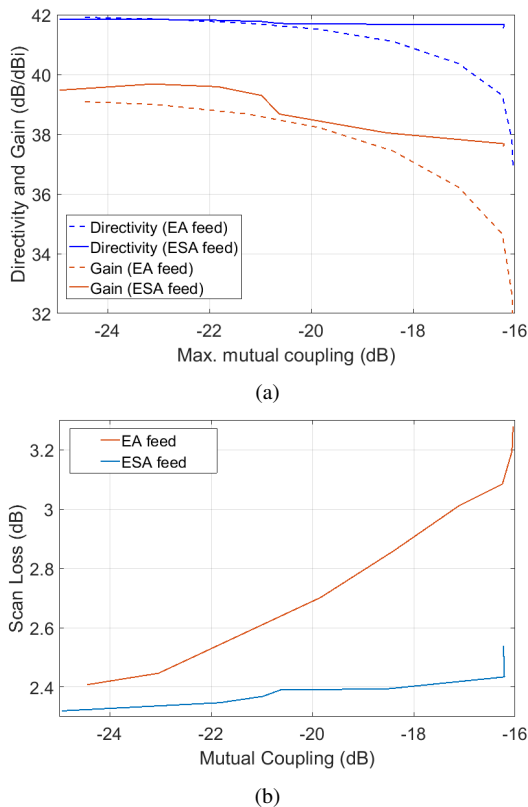


Fig. 6: (a) Bore sight directivity and gain and (b) directivity scan loss comparison of the 5.4° beam of the ILA (feed offset 9.2 mm) fed with mutual coupling varying EA and the ESA feeds.

5 Effects of port impedance mismatch

The characteristic impedance of all elements of the both embedded structures designed in section 3 is 50Ω . In order to emulate the possible mismatch condition introduced by RF switches, the port impedances of the inactive elements i.e. element 2 - 7 of the ESA are varied between 1Ω and 2500Ω while keeping the active element i.e. element 1 port impedance as 50Ω . Element separation distance d of the structures and height h of the parasitic patch is held constant at 2.3 mm and 2 mm, respectively, to achieve maximum mutual coupling. With the varying port impedance of inactive ports from the characteristic impedances, mutual coupling i.e. scattering parameter S_{i1} decreases from -16 dB to -25.6 dB respectively. Almost negligible effect upon the active port impedance matching was observed. Considerable variation on the H-plane cut ($\phi = 0^\circ$) of the radiation pattern was observed as compared to E-plane. Therefore, only the H-plane cut ($\phi = 90^\circ$) of the ESA feed and ILA radiation pattern is demonstrated in this section. Radiation pattern variation starts to saturate after the reflection coefficient magnitudes of the inactive ports exceeds 0.9. The amount of distortion in the feed radiation pattern is dependent upon the feed types and mutual coupling level. The amount of change in the ILA pattern is the function of the feed radiation pattern. In case of ESA feed, the boresight directivity and the first side lobe level (SLL) of the ILA approximately varies 1 dB and 5 dB, respectively, see Figure 7 (a) and (b).

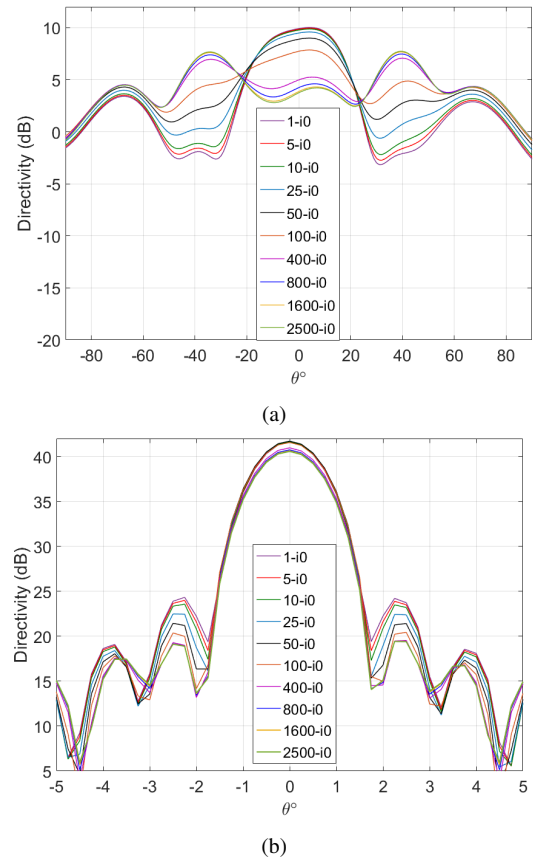


Fig. 7: H-plane ($\phi = 0^\circ$) cut of (a) ESA feed, and (b) the ILA radiation pattern w.r.t. varying real port impedances at inactive ports.

It is likely that the inactive ports impedance are of complex nature. Hence, the inactive ports are assigned with capacitive and inductive impedances. Figure 8 (a) shows that the inductive ports around active element enhances the broadside radiation marginally whereas the capacitive ports reduces it as compared to resistive ports of same amplitude. Consequently, 3 dB variation in SLL of the ILA radiation

pattern can be observed in Figure 8 (b) whereas the boresight directivity changed by 1 dB. The extent of such distortion depends upon the selected feed type.

Until now, impedances of all inactive ports were considered equal. However, each inactive ports can have different impedance values. Therefore, the ESA is initially simulated with various random combinations of the port impedances between 1Ω and 2500Ω . Results showed that the main beam of active element starts to tilt towards the inactive antenna with higher port impedances. Effects of some extreme combinations on the radiation pattern is shown in Figure 8 (c) and (d). With organized and extreme port impedance variation i.e. $(1/1/1/2500/2500/2500) \Omega$ and $(2500/2500/2500/1/1/1) \Omega$ in ports 2/3/4/5/6/7, the main beam tilt can be seen. The extent of beam tilting may vary with the feed type and mutual coupling level between array element. Based on the direction and extent of the feed radiation pattern tilt, the asymmetry of SLL occurs or in worst cases, steering of the ILA mainlobe away from desired direction is possible, see Figure 8 (d).

6 Discussion

Comparison between the far-field radiation pattern of the ILA fed with two different types of feed with similar mutual coupling variation helps to conclude that the feed radiation pattern has critical effects on the ILA performance. Changes in the radiation pattern and the mutual coupling are interrelated phenomena in an antenna array. The amount of mutual coupling and the radiation pattern variation depends upon the selected antenna type. Although the mutual coupling has some undesirable effect in array performance, it could be more important for system level inspection. The mutual coupling is not seen as a good figure of merit alone to evaluate ILA performances. Instead, an evaluation of the feed radiation pattern is required.

Study of the beam steering properties illustrated that scan loss increases. However, the extent of variation depends upon the feed radiation pattern and feed type used.

The variation in the port impedances of the beam-switching array seems to have negligible impact upon the impedance matching and boresight directivity of an ILA. However, slight variation in SLL upto 2 dB was observed based on the feed radiation pattern. Interesting beam-tilting of the feed is seen with the unequal port impedances across the inactive ports of the array.

As the feed designer's point of view, the amplitude and phase of the feed array are critical for the optimum ILA directivity. The feed directivity of approximately 12 dB is desired for optimum directivity and approximately 13 dB for optimum ILA gain performance. Additionally, maximum feed directivity toward boresight i.e. $\theta = 0^\circ$ alone does not ensure optimum ILA directivity and gain. It can only be achieved if maximum feed power is radiated towards collimating surface of the ILA (i.e. $\theta \leq \pm 50^\circ$ in this case). The spherical (undistorted) phase front of the feed antenna that gives equi-phased aperture field is essential to achieve maximum directivity. Mutual coupling level has negligible effects if the radiation pattern remains undistorted. The result shows close correlation between the spillover loss and pattern distortion and consequently the effects on the ILA performance. Therefore, the spillover loss of feed radiation pattern can be used as a simple metric to evaluation pattern distortion.

This study is a numerical analysis of the specific feeds (i.e. EA and ESA) effects on the specific type of lens, 160-mm elliptical ILA, at specific frequency of 73.5 GHz. The simulation tools used in the study is considered to be highly reliable and efficient to estimate the feed radiation pattern and the mutual coupling and further the ILA radiation. It is likely, that the mutual coupling between the array element and the radiation pattern vary w.r.t. element types and frequency range. However, the conclusions of the work is expected to remain for any variation in the mutual coupling and radiation pattern. Although, the experimental verification would improve the reliability of the work, it would be expensive and laborious due to number of feed types used. Therefore, fabrications and measurements are not in the scope of this work. The effects of higher order reflections from the ILA surface on mutual coupling are not considered. In this study,

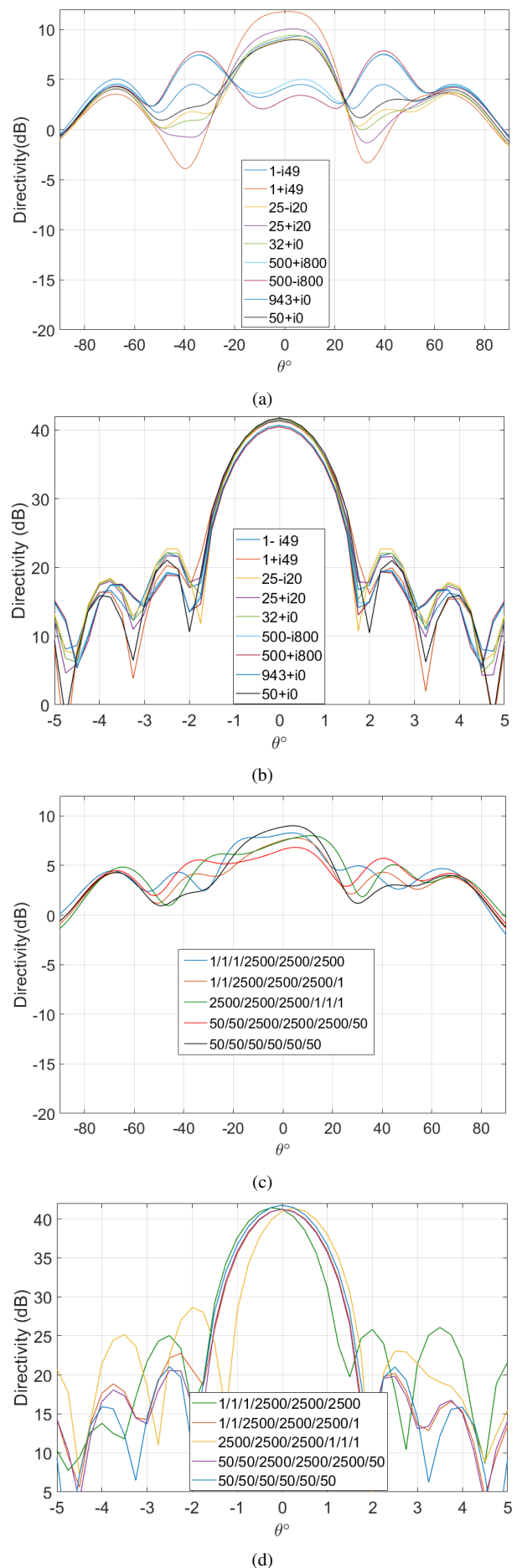


Fig. 8: Radiation pattern variation of ESA and ILA w.r.t. complex port impedance i.e. (a) and (b), and unequal port impedances i.e. (c) and (d), respectively at $\phi = 0^\circ$ (H-plane) cut.

the low permittivity material ($\epsilon_r = 2.31$) is used for the ILA and rays from extension section are not considered for the far-field calculation, thus the effect due to higher order reflections is minimum. However, in case of denser materials, effect of secondary reflections becomes critical.

7 Conclusion

In this work, the effects of mutual coupling and port impedance mismatch of the feed array elements on the ILA performance are numerically studied. Results show that the directivity and radiation pattern of the feed has more impact than the mutual coupling itself. Significant distortion of the feed radiation pattern causes decreased illumination of the ILA collimating surface resulting in the reduced ILA directivity. The ILA directivity and gain can be improved with the feed radiating maximum power towards collimating section with minimum phase distortion. Port impedances mismatch of the adjacent inactive antennas in a beam-switching array have minimal effect on the impedance matching and boresight directivity of the ILA, however some minor variation in the SLL is possible.

8 Acknowledgement

We would like to thank Business Finland for supporting the work through 5WAVE project.

9 References

- [1] Karttunen, A., Ala-Laurinaho, J., Sauleau, R., and Räisänen, A. V.: 'Reduction of internal reflections in integrated lens antennas for beam-steering', *Progress in Electromagnetics Research*, 2013, 134, (10), pp 63–78
- [2] Mozharovskiy A., Artemenko, A., Sevastyanov, A., Ssorin, V. and Maslennikov, R.: 'Beam-steerable integrated lens antenna with waveguide feeding system for 71–76/81–86 GHz point-to-point applications', 2016 10th European Conference on Antennas and Propagation (EuCAP), Davos, Switzerland, April 2016, 1–5
- [3] Ala-Laurinaho, J., Aurinsalo, J., Karttunen, A., Kaunisto, M., Lamminen, A., Nurmiharju, J., Räisänen, A. V., Säily, J., and Wainio, P.: '2-D Beam-Steerable Integrated Lens Antenna System for 5G E -Band Access and Backhaul', *IEEE Transactions on Microwave Theory and Techniques*, 2016, 64, (7), pp 2244-2255
- [4] Karki, S. K., Ala-Laurinaho, J., Viikari, V., and Valkonen, R.: 'Lens antenna design for E-band point-to-point radio links,' 2017 38th Progress in Electromagnetic Research Symposium, St. Petersburg, Russia, May 2017, 1–2
- [5] Gupta, I., and Ksienski, J., : 'Effect of mutual coupling on the performance of adaptive arrays', *IEEE Transactions on Antennas and Propagation* , 1983, 31, (5), pp. 785-791
- [6] Yurduseven , O., Cavallo , D., Neto , A., Carluccio , G., Albani , M.: 'Parametric analysis of extended hemispherical dielectric lenses fed by a broadband connected array of leaky-wave slots', *IET Microwaves, Antennas Propagation*, 2015, 9, (7), pp 611-617
- [7] Vander Vorst, M. J. M., Maagt, P. J. I. de, Herben, M. H. A. J.: 'Scan-Optimized Integrated Lens Antennas', 1997 27th European Microwave Conference , Sept 1997, Jerusalem, Isarel, pp 605-610
- [8] Filipovic D. F., Gearhart, S. S., and Rebeiz, G. M.: 'Double-slot antennas on extended hemispherical and elliptical silicon dielectric lenses', *IEEE Transactions on Microwave Theory and Techniques*, 1993, 41, (10), pp 1738-1749
- [9] Karttunen A., Ala-Laurinaho, J., Sauleau, R., and Räisänen, A. V.: 'Extended hemispherical integrated lens antenna with feeds on a spherical surface', 2013 7th European Conference on Antennas and Propagation (EuCAP), Gothenburg, Sweden, April 2013 , pp 2539-2543
- [10] Komljenovic T., Burum, N., and Sipus, Z.: 'Raytracing analysis of lens antennas - practical approach', 2009 International Symposium ELMAR , Zadar, Croatia, September 2009, pp 313–316
- [11] Van der Vorst, M. J. M., Maagt, P. J. I. de, and Herben, M. H. A. J.: 'Effect of internal reflections on the radiation properties and input admittance of integrated lens antennas', *IEEE Transactions on Microwave Theory and Techniques*, 1999, 47, (9), pp 1696–1704
- [12] Balanis, C. A.: 'Antenna theory: analysis and design' , John Wiley & Sons , Hoboken, New Jersey, 2005.
- [13] Nishiyama, E., Aikawa, M., and Egashira, S.: 'Stacked microstrip antenna for wideband and high gain', *IEE Proceedings - Microwaves, Antennas and Propagation* , 2004, 151, (2), pp. 143-148
- [14] Terret, C., Assailly, S. , Mahdjoubi, K., and Edimo, M.: 'Mutual coupling between stacked square microstrip antennas fed on their diagonal', *IEEE Transactions on Antennas and Propagation*, 1991, 39, (7), pp 1049-1051
- [15] Lamminen, A. E. I., Säily, J., and Vimpari, A. R.: '60-GHz patch antennas and arrays on LTCC with embedded-cavity substrates', *IEEE Transactions on Antennas and Propagation* , 2008, 56, (9), pp. 2865-2874